Deriving a high-resolution record of Greenland glacier discharge

Michalea D. King[12] and Ian M. Howat[12]

1. The Ohio State University, School of Earth Sciences
2. The Byrd Polar and Climate Research Center

ABSTRACT

Ice mass loss from the Greenland Ice Sheet is a major contributor to present-day sea level rise. Some of this mass is lost through the calving of ice from marine-terminating outlet glaciers. This research documents changes in speed and velocity for a large collection of glaciers by assimilating modeled and remotely sensed data. These data are used to derive continuous time series of solid ice discharge for every major glacier in Greenland over the 2000-2016 period. Combined, these records provide a single cumulative time series of the total dynamic ice loss of the GrIS, and reveal a marked seasonality superimposed on long-term trends. These data will allow us to identify regions of the ice sheet most vulnerable to change, and better understand how seasonal variability in ice flux contributes to overall glacier mass-balance, and the health of the ice sheet going forward.

1. INTRODUCTION

Mass loss from the Greenland Ice Sheet (GrIS) is now the single largest cause of sea level rise (Vaughan et al. 2013), contributing nearly 1 mm a^{-1} of global water equivalent over the 2010-2015 period (van den Broeke et al. 2016). Since the mid 1990's, the GrIS has been losing ice at an increasing rate (Rignot et al. 2011; Sasgen et al. 2012; Enderlin et al. 2014) due in part to increased discharge from marine-terminating outlet glaciers (Rignot and Kanagaratnam, 2006; Rignot et al. 2008; Enderlin et al. 2014). Substantial increases in ice discharge observed at large outlet glaciers over periods of months or less (e.g. Joughin et al., 2004; Howat et al. 2005) demonstrated their short term volatility and sensitivity to external drivers, such as ocean circulation (Straneo et al. 2012; Walsh et al. 2012) melt runoff (Joughin et al. 2008; Andersen et al. 2011), and sea ice/mélange conditions near the calving front (Howat et al. 2010; Moon et al. 2015; Bendtsen et al. 2017). Thus, understanding the dynamics of these glaciers requires measurements with a high temporal resolution.

Seasonal variability in glacier velocity has been observed for small samples of glaciers using in-situ GPS units (Joughin et al. 2008; Andersen et al. 2011; Ahlstrøm et al. 2013) and time-lapse photography (Ahn, Y., and Box, J.E., 2010), as well as for larger glacier inventories using TerraSAR-X radar data from 2009 to 2013 (Moon et al. 2014; Moon et al. 2015). Ice sheet-wide, sub-annual observations of discharge that can sufficiently resolve seasonal variability, however, are still needed. Here we present the first continuous monthly record of net ice sheet discharge, derived over the 2000-2016 period.

2. DATA AND METHODS

Here we derive time series of the solid ice discharge (D) for each glacier by integrating the product of glacier thickness (h), ice velocity (v), and ice density (ρ) across the glacier width at the grounded terminus following a similar methodology described in Howat et al. (2011). Observations are sampled along a static profile, i.e. flux gate, oriented perpendicular to the direction of flow and located upstream of the grounding line, immediately inland of the most retreated grounding line. We use same flux gates as Howat et al. (2011) and Enderlin et al. (2014) except in cases where the grounding line had retreated inland of the gate location. Further, while Enderlin et al. (2014) used empirical relationships to estimate cross-sectional area and discharge at glaciers for which only along-flow profiles or no bed topography were available, we use the BedMachine version 3 gridded bed topography dataset (Morlighem et al. 2017), which uses ice thickness and flow speed observations to constrain a mass conservation model. As in prior studies, we assume that changes in the elevation of the glacier bed, due to erosion, deposition and/or lithosphere displacement, are small, as are variations in ice flow velocity with depth in fast flowing (> 1 km/yr) glaciers. Thus, discharge is estimated from the bed topography and repeat measurements of surface elevation and ice flow velocity. Ice velocity and ice thickness, to be discussed in more detail below, are sampled across a flux gate (see Figure 1). A flux gate transect is partitioned into equally-spaced bins approximately 250 meters in width. Transects are sampled at a higher spatial resolution for small glaciers (< 4 km wide), and in cases where increased sampling improves the quality of surface elevation data extraction and processing.

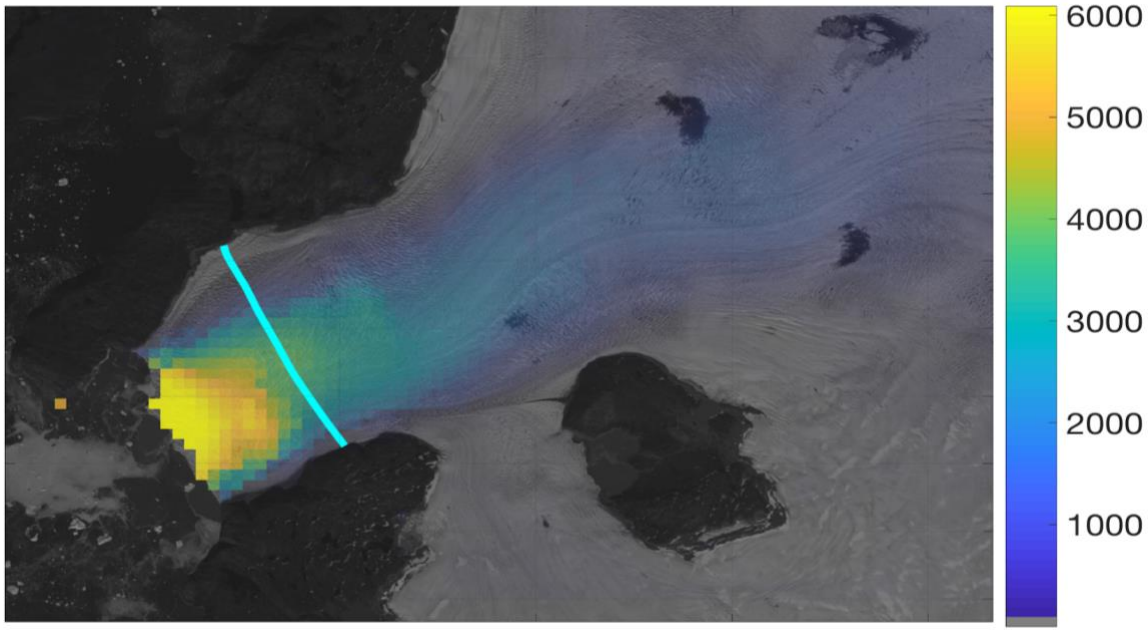

Figure 1: Examples of glacier flux gates (teal) drawn for Store Glacier. Underlying scenes depict orthorectified optical imagery of the glacier termini with an overlying velocity map of ice speeds in July 2016, expressed as m a^{-1}.

2.1 Glacier Velocity

Observations of glacier speed are derived from horizontal velocity maps generated using orthorectified optical imagery from LANDSAT -7, LANDSAT -8, and Advanced Spaceborne Thermal Emission and Reflection radiometer (ASTER) bands 1-3. Ice surface velocity (v) is assumed to be representative of the depth-averaged velocity. Temporal density is improved by integrating multi-sensor, same-track and cross path image pairs (Jeong et al., 2017). Optical observations are augmented by InSAR observations beginning in 2009, obtained from the Terra/TandemSAR-X satellite. Velocity data, extracted along the multiple coordinate points along the glacier flux gate, are initially filtered by the magnitude of the observational error and the corresponding matching ratio parameter. Errors in the optical observations are a product of

the optical imagery quality (noise to pixel ratio), speed of the observed glacier, and number of available optical image pairs. We used a maximum matching ratio threshold of 0.0675 (4 out of 64 successfully matched image pairs), excluding observations with a matching ratio below this threshold from the analysis. The resulting time series, with outliers removed, may still consist of thousands of observational data points due to the high density of multi-sensor, cross-track optical observations.

Despite the high density of optical velocity data, gaps in the time series still exist during winter months when radar-derived glacier speeds are unavailable. A Kalman Filter, a method that has previously been used to estimate height changes in Antarctica from ICESat data (Nguyen et al. 2005), is applied to model reasonable estimates of glacier speed for these missing periods. Modeled ice velocities for missing months are estimated using a linear model of estimated median acceleration for the specific month of interest, derived using a constructed standard seasonality specific to each glacier. To derive the standard seasonality curve, a weighted moving mean filter, weighted by the uncertainties of the respective observations, is first applied to the time series. Next, any existing trends in the monthly-resolved time series, up to a fourth-order polynomial, are removed. Observations in the resulting detrended series are then grouped into bins by month of observation. The standard expected seasonality for each glacier is derived by finding the median value and covariance of each monthly grouping. If no optical or radar data exist for a particular month throughout the time series, a standard monthly value is estimated by extracting the desired monthly solution from a periodic function fit to the available monthly median values. Within the Kalman filter framework, estimates for missing periods are derived by calculating the optimally-interpolated estimate from the two nearest

surrounding observations, with the linear model derived from the standard seasonality curve serving as the initial background state.

2.2 Glacier Ice Thickness

Discharge can also change as a function of time-varying glacier thickness. We find glacier thickness across the flux gate by differencing surface elevation data with a glacial bed topography product, BedMachine v3 (Morlighem et al., 2017), which implements a mass conservation approach based on assimilated available ice thickness and seafloor bathymetry data. We use the same repeat ice surface elevation dataset as Enderlin et al. (2014), extended through 2016, and with the addition of stereoscopic digital elevation models produced from submeter resolution DigitialGlobe Inc. WorldView imagery for the ArcticDEM project (www.arcticdem.org). The DEMs are produced to 2-m resolution and coregistered over stationary (exposed rock) surfaces using the algorithm of Noh and Howat (2014). Following coregistration to remove biases, these data have an accuracy of better than +/-0.5 m (Noh and Howat, 2015). In addition to errors intrinsic to the various surface elevation datasets, systematic errors arise from bed topography and vary spatially across the ice sheet.

2.3 Derivation of Continuous Discharge Time Series

The continuous glacier velocity time series, now comprised of a combination of modelled and observational data, is of a higher temporal resolution than available ice thickness data. For this reason, observations of ice thickness (h) are linearly interpolated onto the temporal space (ti) of glacier velocity (v) observations. A record of solid ice discharge at each glacier is then calculated by summing the discharge at each equally-spaced bin (j), with width w, along the

glacier flux gate (Equation 4, below). A constant density (ρ) of 910 kg m^{-3} is assumed with depth.

$$D_{t_i} = \sum_{j=1}^{n} h_{j,t_i} w_j \vec{v}_{j,t_i} \rho$$

Equation 4

Error in discharge estimates therefore arise from errors in glacier thickness (*he*) and velocity (*ve*) retrievals. total discharge error (*DE*, hereafter to be expressed as 1 standard deviation, $\boldsymbol{\sigma}$), is the sum of random (denoted by subscript *b*) and systematic errors (denoted by subscript *s*). Random error (Equation 5) at each time step is found by summing the errors introduced by both glacier velocities and random errors in ice thickness:

$$DE_{r,t_i} = \sum_{j=1}^{n} h_{,j,t_i} w_j \overrightarrow{ve}_{j,t_i} \rho + + \sqrt{\sum_{j=1}^{n} (he_{r,j,t_i} w_j \vec{v}_{j,t_i} \rho)^2}$$

Equation 5

Systematic errors are a result of biases in bed topography retrievals, and are calculated as:

$$DE_{s,t_i} = \sum_{j=1}^{n} he_{s,j,t_i} w_j \vec{v}_{j,t_i} \rho$$

Equation 6

The discharge time series now include weekly estimates of *D* for periods when data is available, and monthly modeled estimates for periods of missing data. A Monte Carlo Ensemble is performed for each glacier time series to derive the continuous discharge curve, which can be sampled at at equally-spaced intervals. Using the existing estimates of *D* and *DE*, a cubic smoothing spline is fit to the time series. Lastly, continuous mean estimates of *D* and the

standard deviation of solutions at each time step are calculated from the 1000-member ensemble (Sample of resulting time series shown in Figure 2).

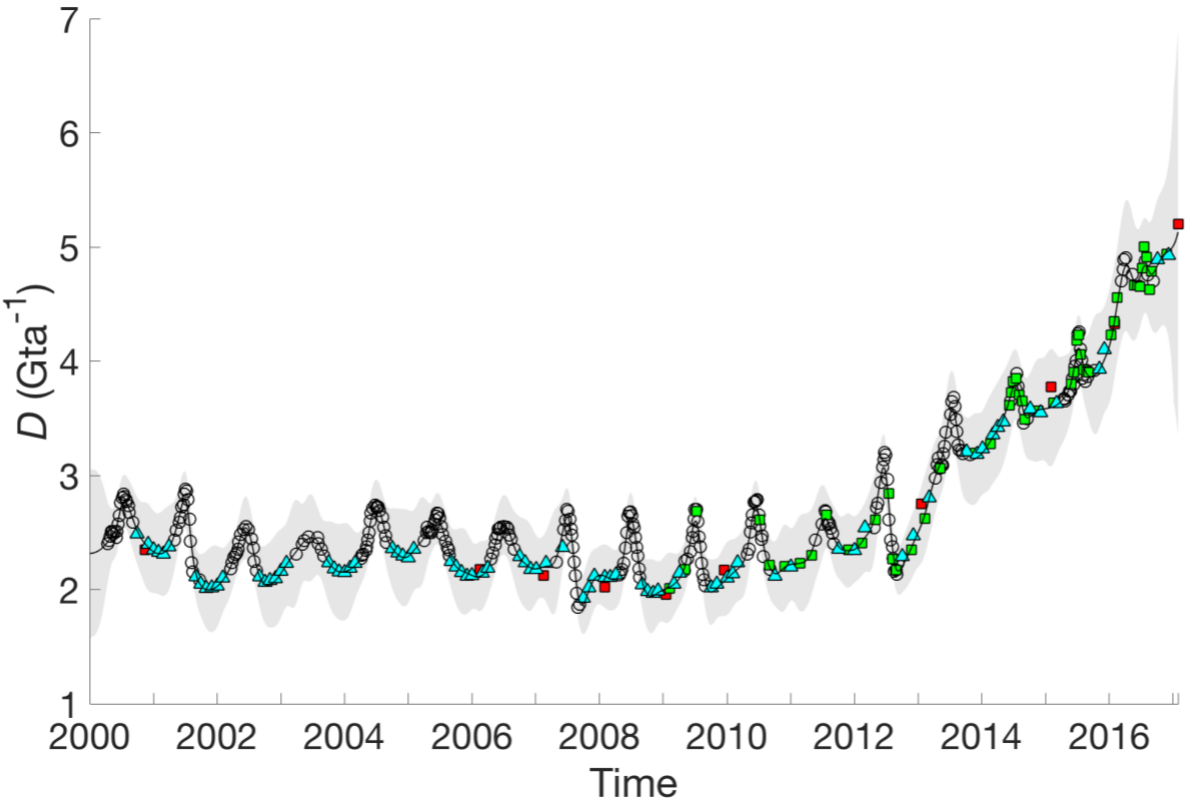

Figure 2: Select solid ice discharge time series for Jensen Glacier. The series shows the resulting continuous time series curve (black), with discharge estimates derived from optical observations (black marker), TerraSAR-X (green squares), RADARSAT-1 and -2 (red squares), and modeled estimates (teal). Shading represents uncertainty (1 $\boldsymbol{\sigma}$). Discharge, $\boldsymbol{D}$, is expressed in Gigatons per year.

3. RESULTS

3.1 Total Ice Sheet Discharge and Mass Balance

The total discharge from all surveyed marine-terminating glaciers for the period 2000 to 2016, displays a clear seasonality, typically peaking in July and reaching an annual minimum in December (Figure 3), superimposed upon multi-year variability. Removing the linearly-interpolated annual means from the time series gives an average seasonal amplitude of 25 Gta^{-1}, or approximately 5% of the mean annual discharge. The seasonal amplitude was largest in 2004, 2005, and 2009, reaching up to 32 Gta^{-1}. Starting from a mean annual discharge of 441 ± 7 Gta^{-1} in 2000, the discharged increased to a maximum of 518 ± 8 Gta^{-1} in late June 2005, mainly due to the accelerations of Kangerdlugssuaq and Helheim glaciers in the east (Howat et al. 2007; Joughin et al. 2008). The rapid decrease in discharge from these two glaciers over the following two years resulted in the smallest observed summer increase in GrIS discharge in 2006, declining to a minimum of 466 ± 6 Gta^{-1} in January 2008. Discharge then increased to a mean annual value of 484 ± 7 Gta^{-1} in 2009, gradually increasing to 493 ± 6 Gta^{-1} in 2015, with a peak summertime value of 510 ± 6 Gta^{-1} in July 2015. Annual discharge declined by 6 ± 12 Gta^{-1} in 2016 due largely to reductions in discharge observed at Køge Bugt and Jakobshavn. Prior to 2013, the seasonal variation in *D* tends to be symmetric, with a single distinct peak and little variability at shorter timescales. The final four years of the record are more variable and include a distinct double peak in 2013 and 2015.

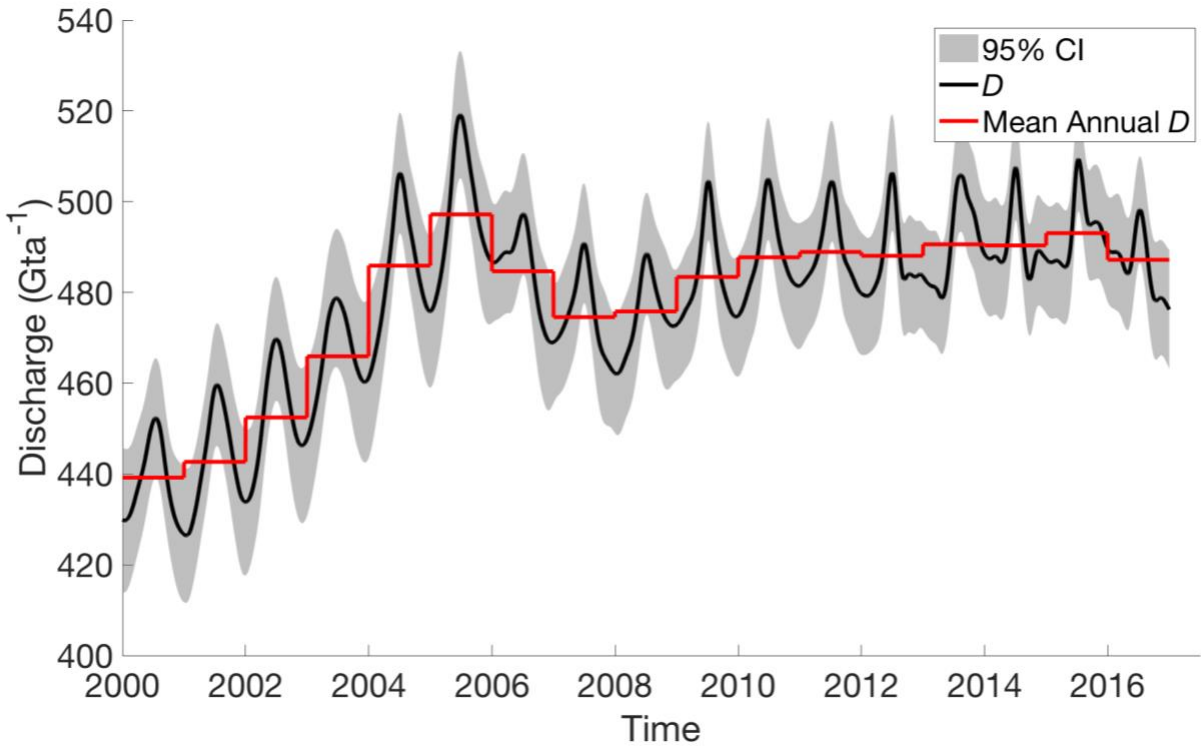

Figure 3: Continuous estimates of discharge (black) for the GrIS for the 2000-2016 study period, expressed as a rate of gigatons per year (Gta^{-1}). Mean annual values are shown in red, with gray shading representing the 95% confidence interval.

The ice sheet's four largest glaciers together account for 25% of the total *D*, and 59% of the cumulative dynamic ice loss, of the GrIS since 2000. Variations in these four glaciers, therefore, dominate variability in total GrIS *D*. Removing the four largest glaciers, however, does not change the relative seasonal amplitude of approximately 5%, indicating that GrIS-wide

seasonality is not dependent on a small sample of glaciers, but rather a ubiquitous seasonal response regardless of glacier size.

3.2 Impact of thinning on the net ice-sheet discharge

Thinning across the flux gate was widespread among the surveyed glaciers, with thinning observed at 89% of glaciers over the study period. These results are consistent with widespread thinning detected in previous studies using aerial photography (Kjeldsen et al. 2015), and radar and laser (Csatho et al. 2014) altimetry. Thinning is observed at all 25 major glaciers (those with mean $D > 5$ Gta^{-1}). The long-term trend in GrIS-wide discharge is dampened by the dynamic thinning of marginal glaciers following prolonged periods of acceleration. Here we quantify the magnitude of this dampening effect by estimating the GrIS-wide discharge calculated by prescribing static ice thicknesses, derived from the beginning of the study period, across the flux gates. We calculate the median flux gate area (integrated ice thickness for each bin across the glacier flux gate) from 2000-2003 to control for short-term variability and combine these values with velocity observations to derive the new scaled discharge time series. We find that thinning imparts a significant impact on the net discharge time series (Figure 4), reducing discharge from the net scaled estimates by approximately 45 Gta^{-1} in 2016. The long-term trend is also dramatically changed, now increasing by 6 Gta^{-2}, and reaching a time series maximum discharge rate of 559 Gta^{-1} in July 2015. Differences between the original and scaled estimates of D also show a subtle seasonality, where differences peak during summertime periods when discharge flux reaches the annual maximum. We find that the scaled series reaches an annual maximum discharge slightly later in the season, although this delay is less than one week for all years. The scaled constant-thickness estimates are not a realistic estimate of the magnitude of D that would be

expected in the absence of widespread thinning, because flow laws govern that glacier velocities would be changed from their observed values. The differences in seasonal variability between the original and scaled estimates, however, suggest that dynamic thinning induced by seasonal glacier acceleration is resolved within the net time series. Without accounting for seasonal thinning, the amplitude of seasonality in the scaled *D* series increased to an average of 28 Gta^{-1}, or approximately 6% of the scaled annual average discharge. These results demonstrate the role of dynamic thinning on both sub-annual and multi-decadal discharge fluxes and reveal the possible discharge biases that may emerge over time if static ice thickness is assumed.

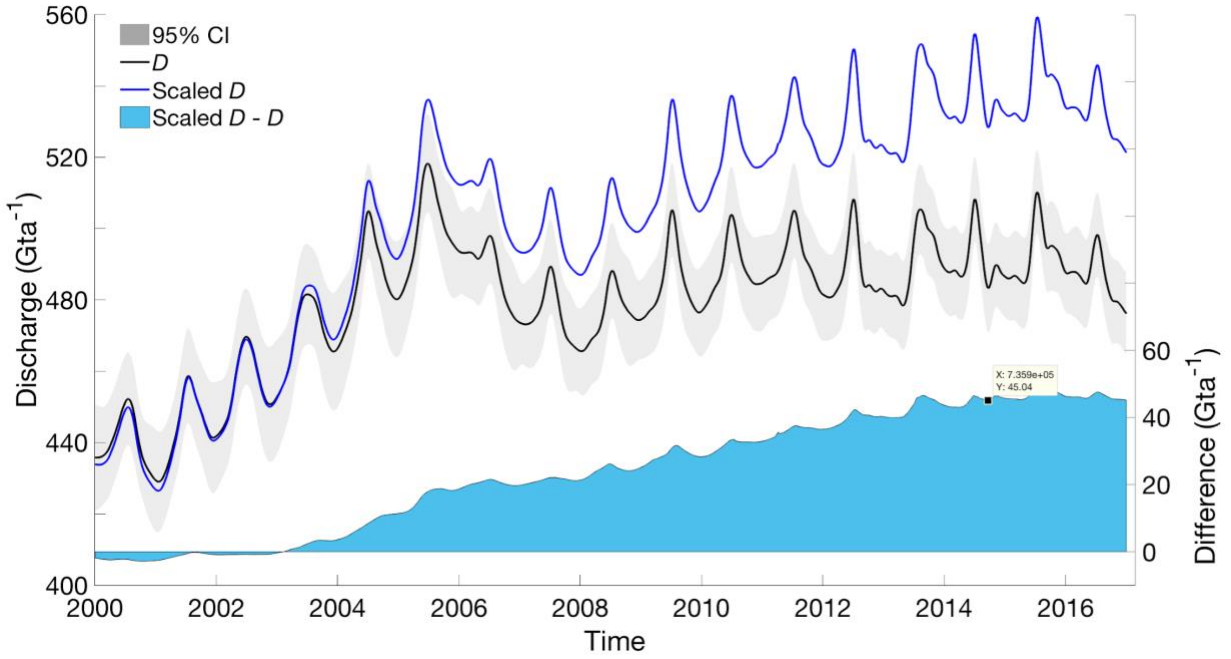

Figure 4: Continuous estimates of net dynamic discharge (black) for the GrIS for the 2000-2016 study period, with discharge estimated scaled for constant glacier thickness in blue. The difference between the original and scaled estimates over time are shaded in light blue.

DISCUSSION AND SUMMARY

We find that our GrIS-wide discharge estimate in 2000 agrees within margins of uncertainty to previous estimates (Rignot et al. 2008) and is approximately 5% and 20% lower than annual estimates derived for 2000 in Enderlin et al. (2014) and Rignot et al. (2011), respectively. These differences likely derive from uncertainties associated with empirical assumptions made in the absence of bed topographic data, uncertainties inherent to bed topography from bedmap3, methodology differences in the processing and filtering of surface elevation data, and uncertainties associated with ice thickness derivations using hydrostatic equilibrium assumptions (Rignot et al. 2011). The monthly temporal resolution of *D* derived here also avoids nonuniform temporal sampling biases, and, once combined with SMB data from RACMO2.3v2, is in excellent agreement with independent estimates of ice sheet mass balance from GRACE. We also derive an adapted discharge record (Figure 4) assuming static glacier thicknesses to show that the recent stabilization in GrIS *D* is due to the impact of dynamic thinning over the study period, which mitigated increases in *D* as glaciers accelerated.

We find a strong and persistent seasonality in discharge of ~5% and find that the relatively symmetrical ice-sheet wide seasonality is becoming more complex, exhibiting a sawtooth-like pattern in the most recent years. This estimate is smaller than previously published values, which estimated seasonal amplitude to be on the order of 8-10%. In the past, seasonality was estimated by either 1.) using a smaller subset of typically larger glaciers with a greater density of observations, which often exhibit enhanced seasonalities compared to the majority of smaller glaciers, or 2.) discharge estimates were scaled by observed variability in glacier velocity, under the assumption that the impact of thickness changes on discharge variability were negligible on short temporal scales.

These results indicate that there is indeed a strong and persistent seasonality exhibited by Greenland's marine terminating glaciers. We also find that a seasonal cycle in *D* is a ubiquitous expression across the ice sheet, although the timing and amplitude of this seasonality may vary between glaciers. Going forward, this record will be compared to other climatic variables such as runoff and mélange and oceanic conditions in an effort to quantity the sensitivity of glacier discharge to these various forcing mechanisms.

REFERENCES

Ahlstrøm, A. P., and Coauthors, 2013: Seasonal velocities of eight major marine-terminating outlet glaciers of the Greenland ice sheet from continuous in situ GPS instruments. *Earth Syst. Sci. Data*, 5, 277–287, doi:10.5194/essd-5-277-2013.

Ahn, Y., and J. E. Box, 2010: Instruments and Methods Glacier velocities from time-lapse photos: Technique development and first results from the Extreme Ice Survey (EIS) in Greenland. *J. Glaciol.*, **56**, 723–734, doi:10.3189/002214310793146313.

Andersen, M. L., M. Nettles, P. Elosegui, T. B. Larsen, G. S. Hamilton, and L. A. Stearns, 2011: Quantitative estimates of velocity sensitivity to surface melt variations at a large Greenland outlet glacier. *J. Glaciol.*, 57, 609–620, doi:10.3189/002214311797409785.

Bendtsen, J., and Coauthors, 2017: Sea ice breakup and marine melt of a retreating tidewater outlet glacier in northeast Greenland (81° N). *Nature*, 1–11, doi:10.1038/s41598-017-05089-3.

Csatho, B. M., and Coauthors, 2014: Laser altimetry reveals complex pattern of Greenland Ice Sheet dynamics. *Proc. Natl. Acad. Sci. U. S. A.*, 111, 18478–18483, doi:10.1073/pnas.1411680112

Enderlin, E. M., I. M. Howat, S. Jeong, M. J. Noh, J. H. Van Angelen, and M. R. Van Den Broeke, 2014: An improved mass budget for the Greenland ice sheet. *Geophys. Res. Lett.*, **41**, 866–872, doi:10.1002/2013GL059010.

Howat, I. M., A. Negrete, and B. E. Smith, 2014: The Greenland Ice Mapping Project (GIMP) land classification and surface elevation data sets. *Cryosphere*, doi:10.5194/tc-8-1509-2014.

Howat, I. M., Y. Ahn, I. Joughin, M. R. Van Den Broeke, J. T. M. Lenaerts, and B. Smith, 2011: Mass balance of Greenland's three largest outlet glaciers, 2000-2010. *Geophys. Res. Lett.*, **38**, 1–5, doi:10.1029/2011GL047565.

Howat, I. M., J. E. Box, Y. Ahn, A. Herrington, and E. M. McFadden, 2010: Seasonal variability in the dynamics of marine-terminating outlet glaciers in Greenland. *J. Glaciol.*, **56**, 601–613, doi:10.3189/002214310793146232.

Howat, I. M., I. Joughin, and T. A. Scambos, 2007: Rapid changes in ice discharge from Greenland outlet glaciers. *Science*, **315**, 1559–1561, doi:10.1126/science.1138478.

Howat, I. M., I. Joughin, S. Tulaczyk, and S. Gogineni, 2005: Rapid retreat and acceleration of Helheim Glacier, east Greenland. *Geophys. Res. Lett.*, doi:10.1029/2005GL024737.

Jeong, S., I. M. Howat, and Y. Ahn, 2017: Improved Multiple Matching Method for Observed Glacier Motion with Repeat Image Feature Tracking. *IEEE Trans. Geosci. Remote Sens.*, **55**, 2431–2441.

Joughin, I., S. B. Das, M. a. King, B. E. Smith, I. M. Howat, and T. Moon, 2008: Seasonal speedup along the western flank of the Greenland Ice Sheet. *Science (80).*, **320**, 781–783, doi:10.1126/science.1153288.

Joughin, I., W. Abdalati, and M. a. Fahnestock, 2004: Large fluctuations in speed on Greenland's Jakobshavn Isbrae glacier. *Nature*, **432**, 2002–2004, doi:10.1038/nature03130.

Kjeldsen, K. K., and Coauthors, 2015: Spatial and temporal distribution of mass loss from the Greenland Ice Sheet since AD 1900. *Nature*, **528**, 396–400, doi:10.1038/nature16183.

Korona, J., E. Berthier, M. Bernard, F. Rmy, and E. Thouvenot, 2009: SPIRIT. SPOT 5 stereoscopic survey of Polar Ice: Reference Images and Topographies during the fourth International Polar Year (2007-2009). *ISPRS J. Photogramm. Remote Sens.*, **64**, 204212

Moon, T., I. Joughin, and B. Smith, 2015: Seasonal to multiyear variability of glacier surface velocity, terminus position, and sea ice/ice melange in northwest Greenland. *J. Geophys. Res. Earth Surf.*, 818–833, doi:10.1002/2015JF003494.

Moon, T., I. Joughin, B. Smith, M. R. Van Den Broeke, W. J. Van De Berg, B. Noël, and M. Usher, 2014: Distinct patterns of seasonal Greenland glacier velocity. *Geophys. Res. Lett.*, **41**, 7209–7216, doi:10.1002/2014GL061836.

Morlighem M. et al., (2017), BedMachine v3: Complete bed topography and ocean bathymetry mapping of Greenland from multi-beam echo sounding combined with mass conservation, *Geophys. Res. Lett.*, **44**, doi:10.1002/2017GL074954.

Nguyen, A. T., and T. A. Herring, 2005: Analysis of ICESat data using Kalman filter and kriging to study height changes in East Antarctica. **32**, 4–7, doi:10.1029/2005GL024272

Noël, B., and Coauthors, 2017: Modelling the climate and surface mass balance of polar ice sheets using RACMO2, Part 1: Greenland (1958-2016). *Cryosph. Discuss.*, 1–35, doi:10.5194/tc-2017-201.

Noh, M. J., and I. M. Howat, 2014: Automated Coregistration of Repeat Digital Elevation Models for Surface Elevation Change Measurement Using Geometric Constraints. *IEEE Trans. Geosci. Remote Sens.*, **52**, 2247–2260, doi:10.1109/TGRS.2013.2258928.

Noh, M.-J., and I. M. Howat, 2015: Automated stereo-photogrammetric DEM generation at high latitudes: Surface Extraction with TIN-based Search-space Minimization (SETSM) validation

and demonstration over glaciated regions. *GIScience Remote Sens.*, **52**, 198–217, doi:10.1080/15481603.2015.1008621.

Rignot, E., J. E. Box, E. Burgess, and E. Hanna, 2008: Mass balance of the Greenland ice sheet from 1958 to 2007. *Geophys. Res. Lett.*, **35**, 1–5, doi:10.1029/2008GL035417.

Rignot, E., I. Velicogna, M. R. Van Den Broeke, A. Monaghan, and J. Lenaerts, 2011: Acceleration of the contribution of the Greenland and Antarctic ice sheets to sea level rise. *Geophys. Res. Lett.*, **38**, 1–5, doi:10.1029/2011GL046583.

Rignot, E., and P. Kanagaratnam, 2006: Changes in the Velocity Structure of the Greenland Ice Sheet. *Science (80-.).*, **311**, 63–86, doi:10.1016/j.cognition.2008.05.007.

Sasgen, I., and Coauthors, 2012: Timing and origin of recent regional ice-mass loss in Greenland. *Earth Planet. Sci. Lett.*, **333**–**334**, 293–303, doi:10.1016/j.epsl.2012.03.033.

Straneo, F., and P. Heimbach, 2013: North Atlantic warming and the retreat of Greenland's outlet glaciers. *Nature*, **504**, 36–43, doi:10.1038/nature12854.

van den Broeke, M. R., E. M. Enderlin, I. M. Howat, P. Kuipers Munneke, B. P. Y. Noël, W. Jan Van De Berg, E. Van Meijgaard, and B. Wouters, 2016: On the recent contribution of the Greenland ice sheet to sea level change. *Cryosphere*, **10**, 1933–1946, doi:10.5194/tc-10-1933-2016.

Vaughan, D. G., and Coauthors, 2013: *Observations: Cryosphere*. 317-382 pp.

Walsh, K. M., I. M. Howat, Y. Ahn, and E. M. Enderlin, 2012: Changes in the marine-terminating glaciers of central east Greenland, 2000-2010. *Cryosphere*, doi:10.5194/tc-6-211-2012.